

Pose Error Effects on Range Sensing

William R. Scott^{†‡}, Gerhard Roth[‡], Jean-François Rivest[†]

[†] Department of Electrical Engineering, University of Ottawa, Ottawa, Canada, K1N 6N5

[‡] Computational Video Group, National Research Council, Ottawa, Canada, K1A 0R6
(william.scott,gerhard.roth)@nrc.ca, rivest@site.uottawa.ca

Abstract

Object reconstruction or inspection using a range camera requires a positioning system to configure relative sensor-object geometry in a sequence of poses. Discrepancies between commanded and actual poses can result in serious scanning deficiencies. This paper provides analytical and experimental characterization of pose error effects for a common type of range camera.

1 Introduction

As illustrated at Fig. 1, the imaging environment for object reconstruction or inspection with active laser-scanning range cameras [1] comprises three main elements: object, range camera and positioning system. Model acquisition involves iterative view planning, sensing, registration and integration. View planning is the task of determining an optimal set of sensor views. Executing the view plan requires physically altering the relative sensor-object pose by means of a positioning system. This may introduce pose error.

Traditional view planning methods use a variety of heuristic techniques relying on surface [5], [13], volume [3], [7] or global [14], [6] scene attributes and generally focus only on object coverage. In performance-oriented reconstruction [9], range data acquisition is based on explicit quality requirements expressed in a model specification - such as sampling precision and density. Performance-oriented view planning requires suitable models of both sensor and positioning system performance. The first should describe the sensor frustum and characterize performance within the calibrated region while the second should describe the positioning system degrees of freedom, range of motion and accuracy within the movement envelope.

This paper summarizes a detailed study [10] of pose error effects on the performance of active laser-scanning range sensors. We address the effects of positioning

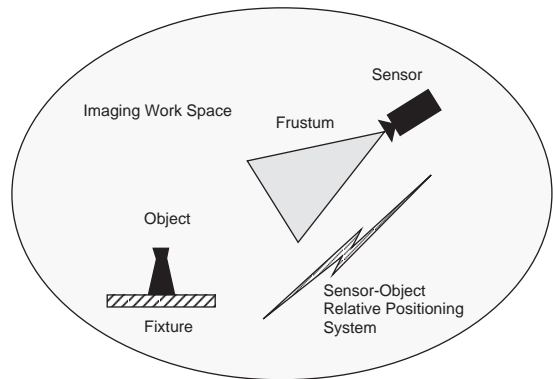


Figure 1: The Geometric Imaging Environment

system inaccuracy in two parts: first an analysis of the impact on a single planned view and then experimental examination of the composite impact on a view plan consisting of multiple views. The analysis is made for a common sensor configuration. Results are generalizable to other range cameras.

2 The Range Sensing Context

2.1 Pose Uncertainty Effects

For a surface point to be measurable by a viewpoint, all model specification requirements must be met at that point. Specifically, for the sensing geometry defined by the viewpoint: the surface point must (1) fall within the sensor frustum, (2) be locally visible by the optical source and receiver and (3) have estimated sampling precision and density within specification.

Unfortunately, pose error adversely impacts all of these requirements. Viewpoint position and orientation are corrupted. Orientation error is particularly troublesome as effects are amplified by range. Image coverage (frustum occupancy), measurement precision

and sampling density are all affected. Visibility can also be affected by the altered viewing geometry.

We can recover a refined pose estimate post-facto by employing suitable registration techniques. However, we are still left with data acquisition differing from that which had been planned. As pose error deteriorates, the computationally intensive view planning phase is progressively compromised - ultimately to be rendered futile. Consequently, there is a need to make the view planning process robust with respect to pose uncertainty resulting from positioning system errors.

2.2 Positioning System Error Model

A variety of positioning systems are in common usage, covering a wide range of accuracy. These include co-ordinate measuring machines (CMMs), translation stages, turntables and robot arms. At the top end, CMMs offer accuracy superior to the best range camera. At the other extreme, robot arms provide good repeatability but poor accuracy relative to the measurement capability of high quality range cameras.

In general, it is difficult to characterize the accuracy of positioning systems with multiple degrees of freedom [11], [12], [2]. Accuracy can also be highly variable over the movement envelope of a given machine. For the purposes of analysis, therefore, we adopt the following simplified but general purpose pose error model. First, we assume calibration has removed systemic errors, leaving only residual stochastic errors. Errors in sensor position, boresight axis and rotation about the boresight (twist) are considered to be independent random processes. Position error is modeled as a 3D vector uniformly distributed in direction and whose magnitude is a zero-mean Gaussian process with standard deviation σ_p . Axis error is modeled by a unit vector uniformly distributed on the surface of a cone centered on the camera boresight where the cone half-angle is a zero-mean Gaussian process with standard deviation σ_a . Twist error is modeled as a zero-mean Gaussian process with standard deviation σ_t . While the model just described is a suitable general purpose framework for analyzing the effects of positioning system error, in practice it will be necessary to develop and apply a specific error model tailored to the type, configuration and movement envelope of each unique positioning system.

2.3 Range Camera Geometry

To illustrate pose error effects, we examine a 3D line-scan range camera. This common configuration (Fig. 2) employs an electronically swept laser scan in the sensor's x-z plane augmented by mechanical motion along

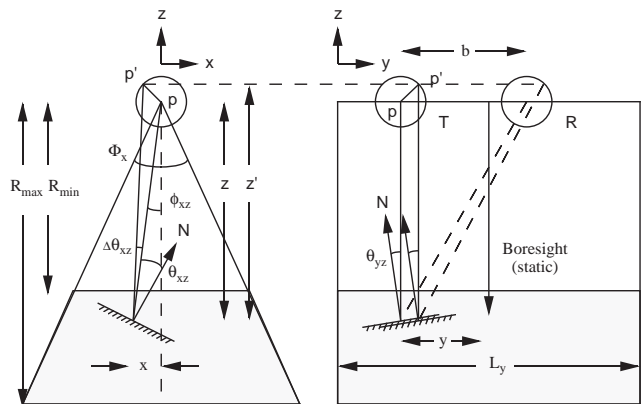


Figure 2: Line-scan Range Camera Geometry

the y-axis. Following convention, the camera axis defines the negative z-axis. The frustum is defined by Φ_x (angular field of view in the x-z plane), L_y (linear scan length in the y-z plane) and R_{min} and R_{max} (minimum and maximum scanning ranges along the z-axis). ϕ_{xz} is the instantaneous laser scan angle. The optical transmitter (laser) and receiver are separated along the y-axis by a distance equal to the optical baseline b .

3 Pose Error and a Single View

3.1 Performance Models

Measurement Precision Our sensor noise model is based on calibration data [4]. The model estimates statistics of the residual random geometric noise as $\hat{\sigma}_x = C_x z, \hat{\sigma}_y = C_y z, \hat{\sigma}_z = C_z z^2$. In the foregoing, $\hat{\sigma}_x, \hat{\sigma}_y, \hat{\sigma}_z$ are the standard deviation estimated noise components along the respective sensor axes, noise coefficients (C_x, C_y, C_z) are derived from calibration data and z is range along the camera boresight.

As noise along the sensor boresight predominates, we use $\hat{\sigma}_z$ as a surrogate for measurement precision. Additionally, estimated sensor noise is modified by an experimentally-derived grazing angle model. Incidence angle effects are most noticeable in the plane of triangulation - that is, the yz-plane, where they generally follow an inverse cosine relationship up to a cut-off angle. Thus, the estimated geometric noise component along the sensor z-axis becomes

$$\hat{\sigma}_z = \frac{C_z z^2}{\cos \theta_{yz}}. \quad (1)$$

To consider the relative impact of pose error, it is

convenient to define relative precision P_{rel} as the ratio of estimated precision in the case of pose error to estimated precision in the error-free case. Then,

$$P_{rel} = \frac{\hat{\sigma}_{z'}}{\hat{\sigma}_z} = \frac{z'^2 \cos \theta_{yz}}{z^2 \cos \theta'_{yz}} \quad (2)$$

where z' and θ'_{yz} are the range and y-z incidence angle as perturbed by pose error.

Sampling Density We use a conservative chord-based estimate for sampling density $\hat{\rho}_z$ where δx and δy are the sampling intervals along the sensor x- and y-axes and δc is the inter-sample chord length.

$$\hat{\rho}_z = \frac{1}{\delta c^2} = \frac{1}{\delta x^2 + \delta y^2} \quad (3)$$

$$\text{where } \delta x = R_{xz} \frac{\Phi_x}{N_x - 1} \frac{1}{\cos \theta_{xz}} \quad (4)$$

$$\text{and } \delta y = \frac{L_y}{N_y - 1} \frac{1}{\cos \theta_{yz}}. \quad (5)$$

In Eq. 4, $R_{xz} = z / \cos \phi_{xz}$ is the slant range, $\Phi_x / (N_x - 1)$ is the angular sampling interval and $1 / \cos \theta_{xz}$ is the inclination effect in the x-z plane. In Eq. 5, $L_y / (N_y - 1)$ is the linear sampling interval and $1 / \cos \theta_{yz}$ is the inclination effect in the y-z plane. Image size is N_x -by- N_y samples.

Using abbreviated notation $C\theta = \cos \theta$ and considering symmetric images ($N = N_x = N_y$), the estimated sampling density is

$$\hat{\rho}_z = \frac{(N - 1)^2 C^2 \theta_{xz} C^2 \theta_{yz}}{R_{xz}^2 \Phi_x^2 C^2 \theta_{yz} + L_y^2 C^2 \theta_{xz}}. \quad (6)$$

Further, an optimized viewpoint equalizes δx and δy . This is achieved by setting stand-off range $z = f_d R_o$, scanning angle $\phi_{xz} = 0$ and adjusting linear scan length to $L_y = f_d R_o \Phi_x$. R_o is the optimum sensor scanning range and f_d is a standoff distance adjustment $f_d = 1 + \delta, \delta \ll 1$. Consequently, for an optimized viewpoint, Eq. 6 becomes

$$\hat{\rho}_z = \frac{(N - 1)^2 C^2 \theta_{xz} C^2 \theta_{yz}}{\Phi_x^2 [R_{xz}^2 C^2 \theta_{yz} + f_d^2 R_o^2 C^2 \theta_{xz}]}. \quad (7)$$

As before, to consider the relative impact of pose error on sampling density, it is convenient to define relative sampling density $D_{rel} = \hat{\rho}_{z'} / \hat{\rho}_z$. Then,

$$D_{rel} = \frac{C^2 \theta'_{xz} C^2 \theta'_{yz}}{C^2 \theta_{xz} C^2 \theta_{yz}} \frac{R_{xz}^2 C^2 \theta_{yz} + f_d^2 R_o^2 C^2 \theta_{xz}}{R_{xz}'^2 C^2 \theta'_{yz} + f_d^2 R_o^2 C^2 \theta'_{xz}}. \quad (8)$$

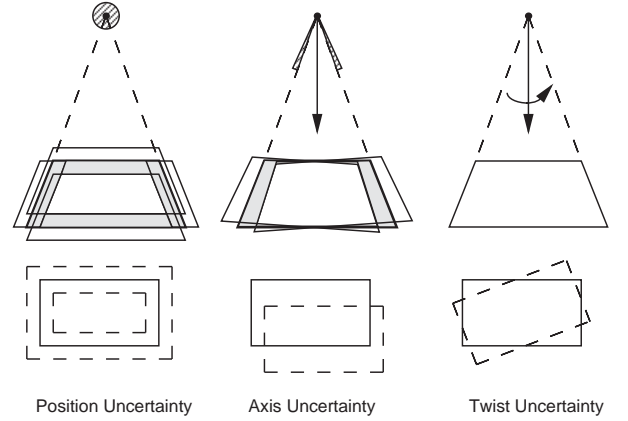


Figure 3: Frustum Erosion with Pose Uncertainty

Frustum Occupancy As illustrated in Fig. 3, pose uncertainty reduces the portion of the frustum that will confidently image a given spatial volume. Pose position error impacts both the effective depth of field (DOF) and field of view (FOV). Pointing uncertainty mainly impacts FOV. Twist error only impacts FOV.

We define the targeted footprint TF as the frustum cross-sectional area at the stand-off range for that viewpoint. Pose error causes the sensor footprint to cover some unplanned regions while losing planned coverage. The coverage gain is of no benefit in planning a single view while the unplanned coverage loss erodes view planning effectiveness. Thus, pose error always reduces and never increases effective coverage of a single scan.

For a line-scan sensor, the targeted footprint is

$$TF = \underbrace{(2f_d R_o T \Phi_2)}_{width} \underbrace{(L_y)}_{length} \quad (9)$$

where $\Phi_2 = \Phi_x / 2$, i.e. half the x-z plane FOV.

To consider the relative impact of pose error on the effective field of view, it is convenient to define the relative targeted footprint $TF_{rel} = TF' / TF$ where TF' is the portion of the perturbed sensor footprint overlapping the targeted footprint.

In considering DOF, only erosion of the effective near-field range limit is of practical concern. For optimum measurement performance, the stand-off range is set at $z = f_d R_o = f_d R_{min}$. Pose error will result in erosion whenever the z-component of frustum change $\delta z > (f_d - 1) R_o$. Therefore, the statistic of interest relative to DOF erosion is the probability $P[\delta z > (f_d - 1) R_o]$.

3.2 Performance Analysis

This section reports the findings of a detailed analytical examination of pose error effects [10]. Briefly, the methodology used was as follows. The effect of each type of pose error on each performance criteria was separately studied. Performance subject to pose error was normalized to the error-free condition. The analysis began by applying error effects to the measurement performance models previously defined. Next, statistics of the underlying random variables were computed. These were used to compute the expected value μ and variance σ^2 for each relative performance measure.

The analysis employed a simple error model based on Gaussian statistics, as previously described. The statistical behavior of real positioning systems is more complex and highly variable between system type and configuration. Pose error is also difficult to characterize and quantify in practice. Furthermore, each pose error effect has been studied in isolation. Multiple types of pose error in combination will interact in a non-linear manner. Nevertheless, while its limitations are acknowledged, the pose error model employed here should form a suitable basis for understanding pose error effects and developing countermeasures.

3.3 Pose Error Effects

Overview Analytical results in pose error variables up to second order effects are presented at Tables 1 and 2. Error effects with non-zero variance are plotted at Fig. 5. Table 3 summarizes key symbols and definitions. The effects of pose position and orientation error are shown. In all cases, performance is relative to the error-free case. The abscissa and ordinate in Fig. 5 are pose error value and relative performance measure, respectively. Average performance and error bars for \pm one and two standard deviations are plotted. In the case of relative targeted footprint (i.e. relative sensor coverage), the curve for $+2$ sigma is clipped at 1.0 because, by definition, pose error only decreases and never increases coverage for a single view.

Precision and Sampling Density The effects of pose error on measurement performance for a single viewpoint are summarized at Table 1 and plotted at Fig. 5(a) and (c). Average relative precision and sampling density are only slightly impacted by pose error but the variance can be significant.

Visibility Occlusion effects depend on several variables, such as the length of the optical baseline, object shape and relative sensor-object pose. The visibility

impact of pose position error will generally be low to nil. An exception is surface regions viewed at incidence angles near threshold or close to occlusion. Axis orientation error causes the optical baseline to wobble. Visibility impacts will generally be low for small axis orientation error. Twist orientation error effects can be quite variable as they cause leveraged movement of the laser source and optical detector in a plane tangential to the targeted region. While small twist errors will have a minor impact in most situations, moderate twist error can introduce significant occlusion problems for complex object shapes.

Sensor Coverage Pose error effects on sensor coverage are particularly problematic as the whole point of view planning is to generate an optimal set of viewpoints with specific coverage and measurability. If actual viewpoint coverage is significantly altered, the entire view planning process can be rendered futile.

Pose error erodes the reliable coverage zone. The effects of pose error on field of view erosion are summarized at Table 2 and are shown at Fig. 5(e),(d) and (f) for pose position, axis and twist error, respectively. The effects can be characterized as low for twist error, high for axis error and moderate-to-high for position error. Axis error is particularly troublesome as coverage perturbations are amplified with standoff range.

Some depth of field erosion occurs with pose position error, Fig. 5 (b). This is easily mitigated by a careful choice of the stand-off distance factor f_d . DOF erosion is negligible for pose orientation error.

4 Multiple Views

In most practical situations, multiple view plans involve a degree of redundant coverage. View planning produces higher levels of image overlap around regions of high shape complexity. Image-based registration requires image overlap and therefore adds redundancy. As the set covering problem is NP-complete [13], practical set covering algorithms are sub-optimal. Longer view plans equate to redundancy. Coverage gain from one view may partially off-set coverage loss from others.

The redundancy phenomena can mask most effects of low levels of pose error in some cases. The phenomena is not amenable to easy analytical treatment due to the large role played by object shape and the fact that view plans are typically short, such that composite coverage statistics are not well behaved.

Carved from stone in the form of a thick shell, the Tsimshian stone mask (Fig. 4), a masterpiece of north-west coast art in the collection of the Canadian Museum



Figure 4: Tsimshian Stone Mask

of Civilization, is an interesting object to illustrate the effects of pose error on a view plan consisting of multiple views. A view plan of five views was computed by our modified measurability matrix technique [8] for the back of the mask. This region is a challenge due to the steep cavity walls and presence of several smaller cavities within the segment. The view plan was evaluated by the experimental process described in [9].

Fig. 6 shows pose error effects for position, axis and twist orientation errors plus their cumulative effect in combination. Average performance and error bars for \pm one standard deviation are shown. Partial-to-complete masking of pose error effects can be noted at low error levels, followed by a rapid decrease in average measurability and rapid increase in measurability variance with pose error deterioration. The data illustrates that, at low pose error levels, range scanning benefits from view plan redundancy while moderate to high levels of pose error result in unpredictable scanning performance. The penalty for coverage failure is typically high for object reconstruction tasks as the imaging team may have left the site or the object may no longer be readily available by the time coverage gaps or measurability deficiencies are discovered. Thus, the unpredictable impact of pose error on multiple view sets may be unacceptable. Effects with simpler object shape will be more severe due to reduced viewpoint correlation.

5 Conclusions

High performance 3D object reconstruction or inspection commences with a model specification requiring views (range images) to pass specific criteria for sam-

pling precision and density, visibility and frustum occupancy. Unfortunately, positioning system errors negatively impact all of these requirements, with the severity generally being in the order of frustum occupancy, measurement variation and occlusion. Additionally, pose error imposes an image-based registration constraint which increases the length of the view plan and model reconstruction time. Finally, pose uncertainty exacerbates collision avoidance planning.

Consequently, view planning requires both sensor and positioning system error models. It is clearly pointless to attempt subtle view planning optimization beyond the precision of the positioning system. This paper has analytically and experimentally characterized pose error effects on a common type of range camera. Future work will examine pose error countermeasures.

References

- [1] P. J. Besl. Range image sensors. In J. Sanz, editor, *Advances in Machine Vision*. Springer-Verlag, New York, 1989.
- [2] P. Cauchick-Miguel, T. King, and J. Davis. CMM verification: A survey. *Measurement*, 17(1):1–16, 1996.
- [3] C. Connolly. The determination of next best views. In *Proc. IEEE Int. Conf. on Robotics and Automation*, pages 432–435, 1985.
- [4] S. El-Hakim and J.-A. Beraldin. Configuration design for sensor integration. In *Proc. Videometrics IV, SPIE, Philadelphia, Pennsylvania*, volume 2598, pages 274–285, 25–26 October 1995.
- [5] J. Maver and R. Bajcsy. Occlusions as a guide for planning the next view. *IEEE Trans. PAMI*, 17(5):417–433, May 1993.
- [6] R. Pito. A sensor based solution to the next best view problem. In *Proc. Int. Conf. on Pattern Recognition*, pages 941–945, August 1996.
- [7] M. Reed, P. Allen, and I. Stamos. Automated model acquisition from range images with view planning. In *Proc. IEEE Conf. Vis. Pat. Rec., San Juan, Puerto Rico*, pages 72–77, June 17–19 1997.
- [8] W. Scott, G. Roth, and J.-F. Rivest. Performance-oriented view planning for automatic model acquisition. In *31st Int. Sym. on Robotics, Montreal*, pages 314–319, May 2000.
- [9] W. Scott, G. Roth, and J.-F. Rivest. View planning for multi-stage object reconstruction. In *14th Int. Conf. on Vision Interface, Ottawa*, pages 64–71, June 2001.
- [10] W. Scott, G. Roth, and J.-F. Rivest. View planning with pose error. Technical Report NRC-44195, National Research Council of Canada, Institute for Information Technology, May 2001.
- [11] Y. Shin and Y. Wei. A statistical analysis of positional errors of a multi-axis machine tool. *Precision Engineering*, 14(3):139–146, July 1992.
- [12] J. Soons, F. Thomas, and P. Schellekens. Modeling the errors of multi-axis machines: A general methodology. *Precision Engineering*, 14(1):5–19, July 1992.
- [13] G. Tarbox and S. Gottschlich. Planning for complete sensor coverage in inspection. *Computer Vision and Image Understanding*, 61(1):84–111, January 1995.
- [14] X. Yuan. A mechanism of automatic 3D object modeling. *IEEE Trans. PAMI*, 17(3):307–311, March 1995.

Measurement	Pose Position Error	Pose Axis Error	Pose Twist Error
Precision	$\mu_{P_{rel}} = 1 + \frac{1}{3f_d^2} \frac{\sigma_p^2}{R_o^2}$ $\sigma_{P_{rel}}^2 = \frac{4}{3f_d^2} \frac{\sigma_p^2}{R_o^2}$	$\mu_{P_{rel}} = 1 - \frac{3\sigma_a^2}{4}$ $\sigma_{P_{rel}}^2 = 0$	$\mu_{P_{rel}} = 1$ $\sigma_{P_{rel}}^2 = 0$
Sampling Density	$\mu_{D_{rel}} = 1 + \frac{1}{3f_d^2} \frac{\sigma_p^2}{R_o^2}$ $\sigma_{D_{rel}}^2 = \frac{2}{3f_d^2} \frac{\sigma_p^2}{R_o^2}$	$\mu_{D_{rel}} = 1 - \frac{\sigma_a^2}{4}$ $\sigma_{D_{rel}}^2 = 0$	$\mu_{D_{rel}} = 1$ $\sigma_{D_{rel}}^2 = 0$

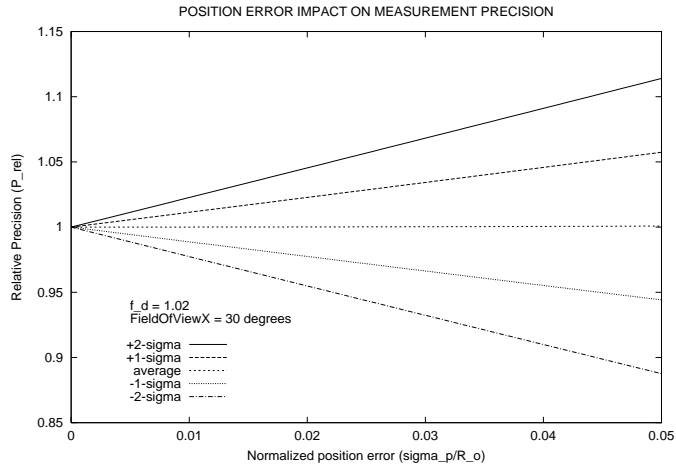
Table 1: Single View Pose Error Measurability Effects: Line-scan Sensor

Error	Field of View Erosion	Depth of Field Erosion
Position	$\mu_{TF_{rel}} = 1 - \frac{(\Phi_x T \Phi_2 + \Phi_x + 2T \Phi_2)}{2f_d \Phi_x T \Phi_2} \sqrt{\frac{2}{3\pi}} \frac{\sigma_p}{R_o} + \frac{(T \Phi_2 + 1)}{3\pi f_d^2 \Phi_x T \Phi_2} \frac{\sigma_p^2}{R_o^2}$ $\sigma_{TF_{rel}}^2 = \frac{(\Phi_x T \Phi_2 + \Phi_x + 2T \Phi_2)^2}{4f_d^2 \Phi_x^2 T^2 \Phi_2} \left(\frac{\pi - 2}{3\pi} \right) \frac{\sigma_p^2}{R_o^2}$	$P[p_z > (f_d - 1)R_o] = 1 - \Phi\left[\frac{\sqrt{3}(f_d - 1)}{(\sigma_p/R_o)}\right]$
Axis	$\mu_{TF_{rel}} = 1 - \frac{(\Phi_x + 2T \Phi_2)}{\pi T \Phi_2 \Phi_x} \sqrt{\frac{2}{\pi}} \sigma_a + \frac{\sigma_a^2}{2\pi T \Phi_2 \Phi_x}$ $\sigma_{TF_{rel}}^2 = \frac{\sigma_a^2}{8\pi^3 T^2 \Phi_2 \Phi_x^2} [(4T^2 \Phi_2 + \Phi_x^2)(\pi^3 - 16) + 8T \Phi_2 \Phi_x (\pi^2 - 8)]$	$P[\alpha > \frac{(f_d - 1)}{f_d \Phi_2}] = 1 - \Phi\left[\frac{(f_d - 1)}{f_d \Phi_2 \sigma_a}\right]$
Twist	$\mu_{TF_{rel}} = 1 - \frac{\Phi_x^2 + 4T^2 \Phi_2}{8\Phi_x T \Phi_2} \sqrt{\frac{2}{\pi}} \sigma_t + \frac{\sigma_t^2}{2}$ $\sigma_{TF_{rel}}^2 = \frac{(\Phi_x^2 + 4T^2 \Phi_2)^2}{64\Phi_x^2 T^2 \Phi_2} \left(\frac{\pi - 2}{\pi} \right) \sigma_t^2$	nil

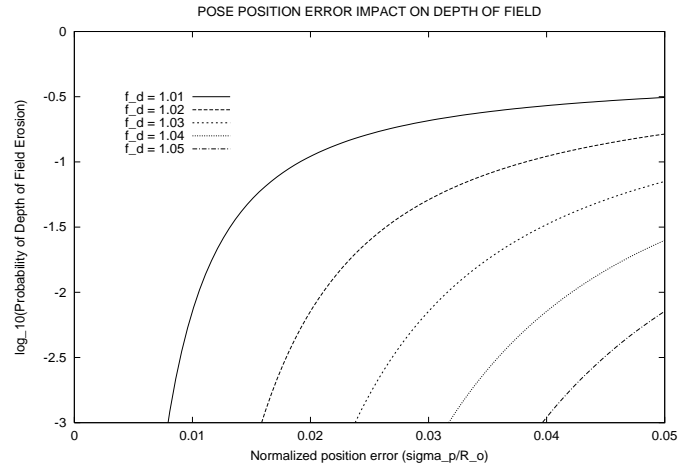
Table 2: Single View Pose Error Coverage Effects: Line-scan Sensor

Symbol	Definition
$P_{rel}, D_{rel}, TF_{rel}$	Relative measurement precision, sampling density, targeted footprint (error vs. error-free)
$\sigma_p, \sigma_a, \sigma_t$	Pose uncertainty standard deviation for position, axis, twist
R_o	Optimum sensor scanning range
f_d	Sensor standoff distance factor $f_d = 1 + \delta$, $\delta \ll 1$
$\Phi_x, T \Phi_2$	Sensor field of view in the scanning plane; $T \Phi_2 = \tan \Phi_2 = \tan \Phi_x / 2$
L_y	Sensor linear scan length along y-axis
N_x, N_y	Number of range image samples in x- and y-axes
p_x, p_y, p_z	Pose position error in x-, y- and z-axes
α	Pose axis error cone half-angle
$\Phi[z]$	Normal distribution function $\Phi[z] = \frac{1}{\sqrt{2\pi}} \int_{-\infty}^z e^{-u^2/2} du$

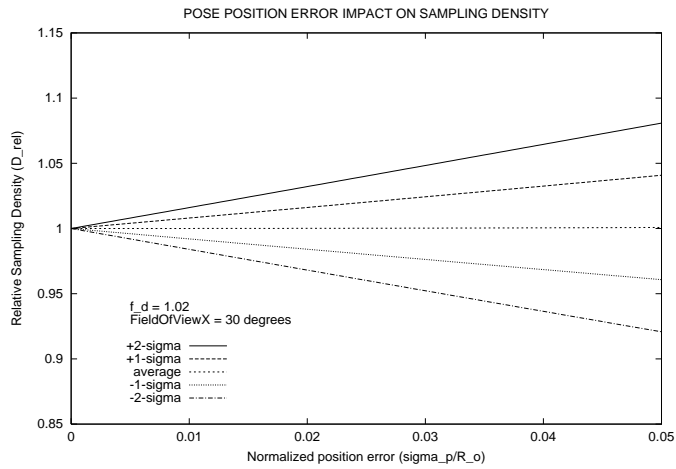
Table 3: Key Symbols and Definitions



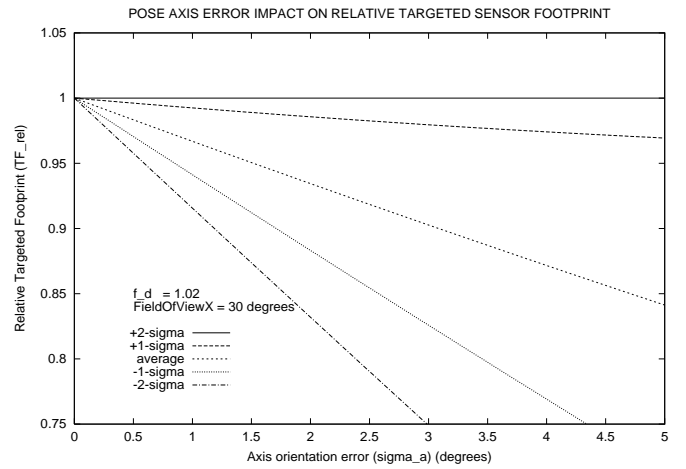
(a)



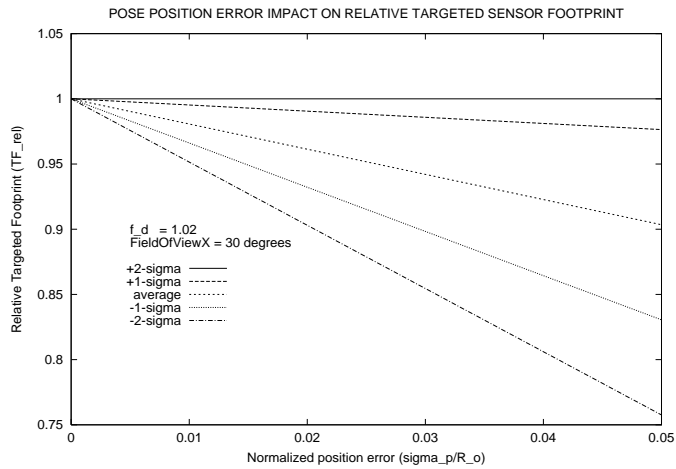
(b)



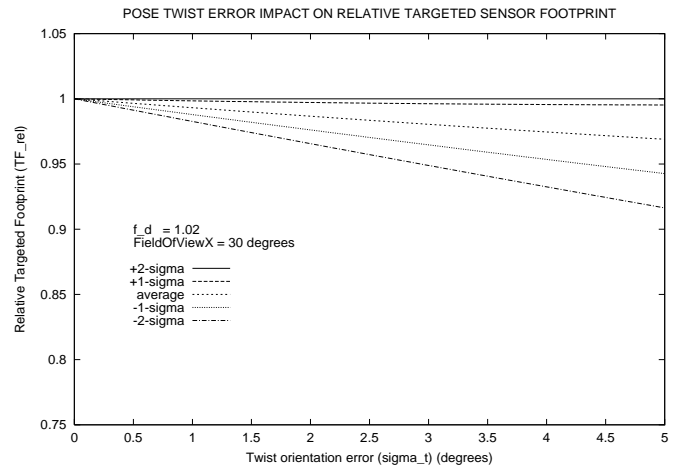
(c)



(d)



(e)

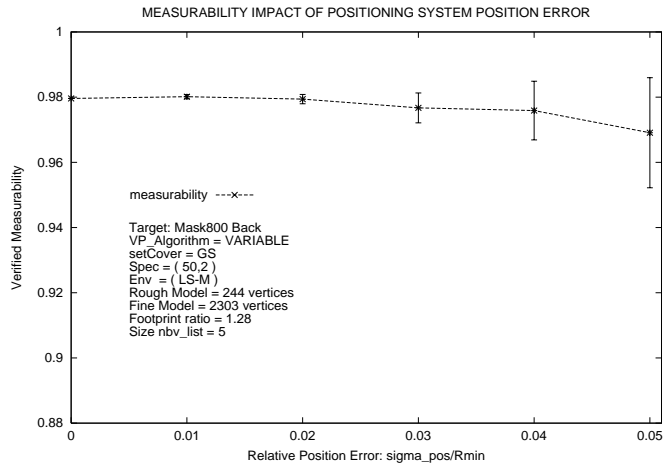


(f)

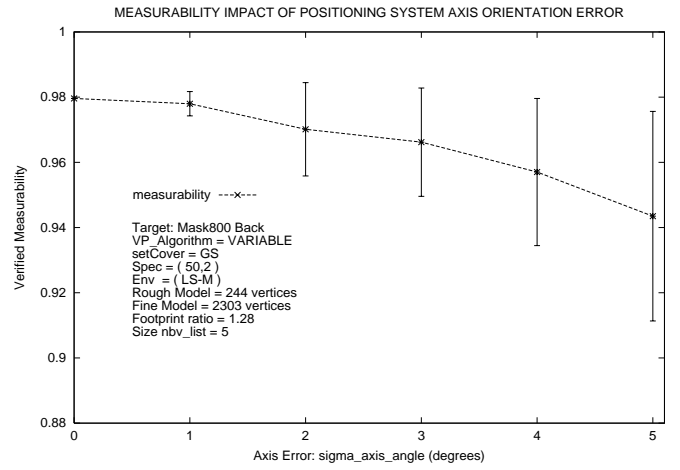
Position error - precision, density, FOV

Position error - DOF; Axis error - FOV; Twist error - FOV

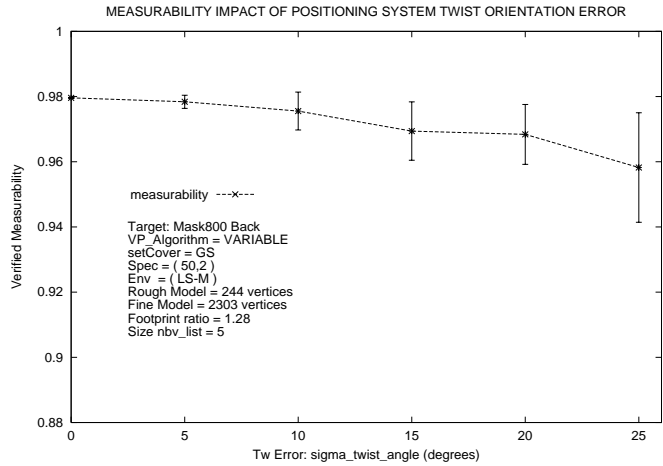
Figure 5: Single View Pose Error Effects



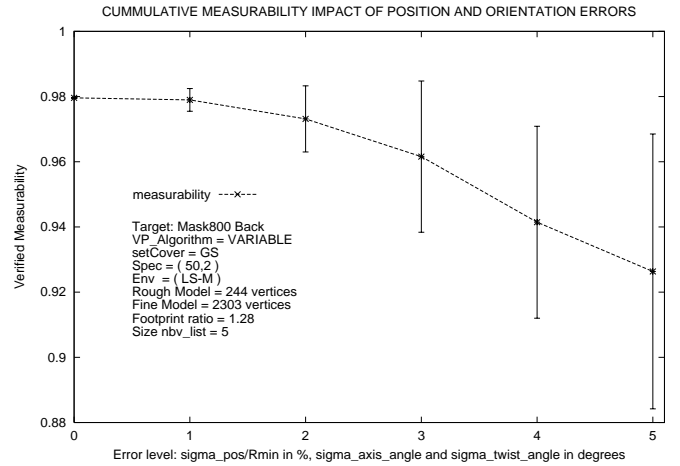
(a)



(b)



(c)



(d)

Figure 6: Multiple View Pose Error Effects - Mask Rear Segment